Contents lists available at ScienceDirect

Journal of Controlled Release

Expediting 3D printed medication development using vacuum compression moulding

Anna Kirstine Jørgensen [a], Ye Chan Oh [a], Hanxiang Li [a], Daniel Treffer [b], Maryam Parhizkar [a], Alvaro Goyanes [a,c,d,e,*], Abdul W. Basit [a,d,*]

[a] *Department of Pharmaceutics, UCL School of Pharmacy, University College London, 29-39 Brunswick Square, London WC1N 1AX, UK*
[b] *MeltPrep GmbH, Nikolaiplatz 4/3, 8020 Graz, Austria*
[c] *Departamento de Farmacología, Farmacia y Tecnología Farmacéutica, I+D Farma (GI-1645), Facultad de Farmacia, Instituto de Materiales (iMATUS) and Health Research Institute of Santiago de Compostela (IDIS), Universidade de Santiago de Compostela, 15782 Santiago de Compostela, Spain*
[d] *FABRX Ltd., Henwood House, Henwood, Ashford, Kent TN24 8DH, UK*
[e] *FABRX Artificial Intelligence, Carretera de Escairón, 14, Currelos (O Saviñao), CP 27543, Spain*

ARTICLE INFO

ABSTRACT

Three-dimensional printing (3DP) is a disruptive technology for producing medications tailored to individual patients, with fused-deposition modelling (FDM) being one of the most established technologies for clinical implementation. However, obtaining FDM pharma-ink (drug-loaded filaments) of consistent diameter may be challenging and time consuming by hot melt extrusion. Additionally, to implement non-destructive quality control methods for 3DP tablets requires producing tablets containing varying levels of active pharmaceutical ingredient for model calibration. Some of these levels may not be possible to manufacture due to impaired formulation processability. Here, vacuum compression moulding (VCM) melt-processing was deployed for assessing two aims for 3DP of personalised oral tablets. First, as a novel small-scale production method for dimensionally accurate pharma-ink, and second, accomplishing non-destructive dose verification in 3DP tablets with a model derived from VCM object samples acting as 3DP tablet surrogates. Tablets containing 10, 20, and 30 mg tamoxifen, a drug currently being progressed in 3DP clinical trials, were accurately printed with the developed pharma-ink, with mass and drug content variations within European and U.S. pharmacopoeia specifications. Release profiles were equal between tablet sizes. For the first time, the feasibility of cylindrical VCM objects as tablet surrogates was demonstrated for non-destructive near-infrared (NIR) dose determination in 3DP tablets. The NIR model calibrated with VCM samples displayed excellent linearity and robustness ($R^2 = 0.997$ and $R^2_{cross\ validation} = 0.996$) with no statistical difference in predicted tamoxifen dose for the tablets as compared to high performance liquid chromatography. This work demonstrates the synergies between VCM and FDM printing for expediting the development of personalised oral medicines with enhanced material sustainability.

1. Introduction

Three-dimensional printing (3DP), also known as additive manufacturing technology, has experienced considerable interest, including for healthcare applications, over the past decade. For pharmaceuticals, 3DP is an enabling technology for personalised medicines to produce bespoke medicines of specific doses and with unique product characteristics such as drug release rates tailored to individual patients or patient groups [1–4].

Multiple 3DP technologies have been researched for production of medicines, although only some technologies are currently in scope for clinical applications due to their use of 'generally regarded as safe' (GRAS) materials and common pharmaceutical excipients. Among these are extrusion-based technologies including fused deposition modelling (FDM) [5], direct powder extrusion (DPE) [6], and semisolid extrusion (SSE) [4]. All three rely on the extrusion of drug-loaded materials (pharma-ink) which for DPE and FDM are thermoplastic powder mixtures or filaments, respectively [7,8], and for SSE a semisolid matrix [9]. The first clinical studies assessing patient acceptability and efficacy of 3DP oral tablets (printlets) have already been published with more underway [10–14].

One of the most researched 3DP technologies for production of

personalised printlets is FDM. Early methods of FDM pharma-ink production included soaking of commercial thermoplastic filaments in drug-laden solutions [15,16], although current standard practice is through hot-melt extrusion (HME) technology to incorporate the active pharmaceutical ingredient (API) within the polymeric matrix [17]. Obtaining an FDM pharma-ink of consistent diameter, typically 1.75 mm, is crucial to achieve printlets of consistent size and quality and to prevent an interrupted 3DP process [17–19]. For HME, interchangeable die sizes and conveyor belt setups to transport the pharma-ink from the extrusion die at a constant rate are employed for this [19–21]. The process parameters (i.e. temperature, screw speed, and die size) are inherently formulation dependent [22]. However, optimisation of this process tends to be heavily time consuming whilst generating excess waste, and even so, obtaining appropriate pharma-ink from HME may not always be possible for different formulation compositions [23].

A very recent expansion of the vacuum compression moulding (VCM) technology has emerged for small-scale production of FDM pharma-ink of up to one meter in length [24]. Compared to HME, a single formulation composition can be tested with only about a tenth of the material required. VCM as a technology relies on the compression of materials through applied vacuum pressure and temperature to generate homogenously fused samples [25,26]. For FDM pharma-ink manufacture via VCM, a formulation is loaded into a feed chamber connected to a 1.75 mm internal diameter tube system which then fills with the formulation under the application of vacuum and heat, ensuring a pharma-ink of exactly 1.75 mm diameter throughout [27]. Besides offering smoother and more material-sparing workflows for developing FDM pharma-inks, the VCM technology could also have important implications for FDM pharma-ink production in settings where operating a HME would be infeasible or inconvenient, i.e. for clinical trials with limited API supply, hospitals handling toxic and hazardous APIs for 3DP, or due to HME setup volume requirements.

A key factor required for full clinical implementation of 3DP for completely personalised medicines is quality control (QC) [28]. Unlike traditional pharmaceutical manufacturing, 3DP for personalised medicines is not focused on mass manufacturing [29]. Instead, its potential for advancing personalised pharmaceutical therapy lies in the versatility of producing small-scale and individualised dosage forms as and when needed, hence conventional QC frameworks remain unsuitable [28,30]. Both the UK Medicines and Healthcare products Regulatory Agency (MHRA) [31], U.S. Food and Drug Administration (FDA) [32,33], and European Medicines Agency (EMA) [34,35] have been actively engaging in conversation on advancing frameworks for distributed manufacturing of medicines and medicines produced at the point-of-care, i.e. by adopting a risk-based approach.

Non-destructive QC methods for 3DP printlets have been researched, including vibrational spectroscopic techniques such as near-infrared (NIR) and Raman spectroscopy for the prediction of various quality attributes [36,37], i.e. quantitation of API within each printlet [38–41]. Preparation of a calibration model of printlets containing varying levels of API and excipients through chemometric modelling for the spectroscopic quantitation is required [42]. Maintaining identical process parameters for the calibration samples, i.e. temperature, as for the developed printlets undergoing spectroscopic analysis can be challenging due to the high dependency on formulation composition. Thus, calibration printlets may display varying resolution due to poorer pharma-ink printability at the employed parameters or inconsistencies in pharma-ink diameter due to altered extrudability for HME. Even if extrudability and printability are not significantly reduced for the different calibration formulations, the entire process of producing a pharma-ink and several printlets per API concentration is labour-, time-, and material consuming.

The aims of this work were two-fold: First, to investigate the novel VCM technology for pharma-ink production for FDM printing of personalised printlets (3DP tablets) containing tamoxifen. Tamoxifen is used to treat women of non-menopausal states recovering from hormone-receptor positive breast cancer. Due to its extensive hepatic metabolism by the Cytochrome P450 2D6 enzyme (CYP2D6) and inter-patient variation in CYP2D6 expression and activity, patients would benefit from tailored doses of tamoxifen enabled by 3DP [43]. Second, this work sought to investigate the feasibility of developing a quantitative NIR calibration model derived from 8 mm cylindrical VCM objects produced at similar processing temperatures to the printlets as a surrogate model for dose verification of tamoxifen in the developed printlets.

2. Materials and methods

2.1. Materials

Tamoxifen citrate (TC) (MW: 563.6 g/mol) was obtained from Hepartex® (Saint-Cloud, France), hydroxypropylcellulose (Klucel ELF; MW: 40,000) and polyvinylpolypyrrollidone (Polyplasdone-XL) from Ashland Industries Europe GmbH (Schaffhausen, Switzerland), and D-Mannitol from Scientific Laboratory Supplies Ltd. (Nottingham, United Kingdom). Sodium phosphate monobasic monohydrate (NaH$_2$PO$_4$·H$_2$O), magnesium stearate (MgSt) (technical grade), *N,N*-dimethyloctylamine (DMOA), acetonitrile (ACN), and 5 M hydrochloric acid (HCl) were purchased from Sigma Aldrich (Gillingham, United Kingdom) while phosphoric acid (for HPLC) was purchased from Thermo Fisher Scientific (Cheshire, United Kingdom). Materials were used as received unless otherwise stated.

2.2. Methods

#### 2.2.1. Formulation preparation

The formulation consisted of TC and excipients according to Table 1. Klucel ELF and Polyplasdone-XL were dried in an oven at 50 °C for 24 h prior to formulation preparation. All excipients and TC were weighed out accurately and mixed for five minutes using a mortar and pestle. Physical mixtures (PM) were made in batches of 5 g.

2.2.2. Preparation of pharma-ink

The pharma-ink, in this case drug loaded filaments, were prepared using VCM and a filament moulder systems (MeltPrep GmbH, Graz, Austria). Firstly, ca. 2.3 g of formulation was transferred to the VCM Disc Tool D25 (25 mm diameter) lined with polytetrafluoroethylene (PTFE) foils (MeltPrep GmbH, Graz, Austria) and compressed at 110 °C under vacuum for 5 min. The compressed disc was cooled to room temperature under continued vacuum. The resulting VCM disc was placed inside a PTFE lined D25 (25 mm diameter) feed chamber for the filament moulder connected to a PTFE tube of 1.75 mm internal diameter (MeltPrep GmbH, Graz, Austria) fitted inside the filament moulder channel. The filament was manufactured at 130 °C and vacuum pressure for 20 min and cooled to room temperature under continued application of vacuum. Cooled filament was liberated from the PTFE tube by passing through a tube cutter (MeltPrep GmbH, Graz, Austria). The equipment produces pharma-ink of up to 1 m in length, and ca. 90 cm long pharma-ink was produced per batch. An overview of the working principles of the instrument have been provided in Fig. 1. The diameter of the prepared filament was validated using a digital Vernier calliper (GNW

Table 1

Formulation composition for TC pharma-ink preparation via VCM filament moulder.

Component	Concentration (% *w/w*)	Mass for 5 g formulation (g)
TC	25	1.25
Klucel ELF	40	2
D-Mannitol	15	0.75
Polyplasdone-XL	15	0.75
MgSt	5	0.25
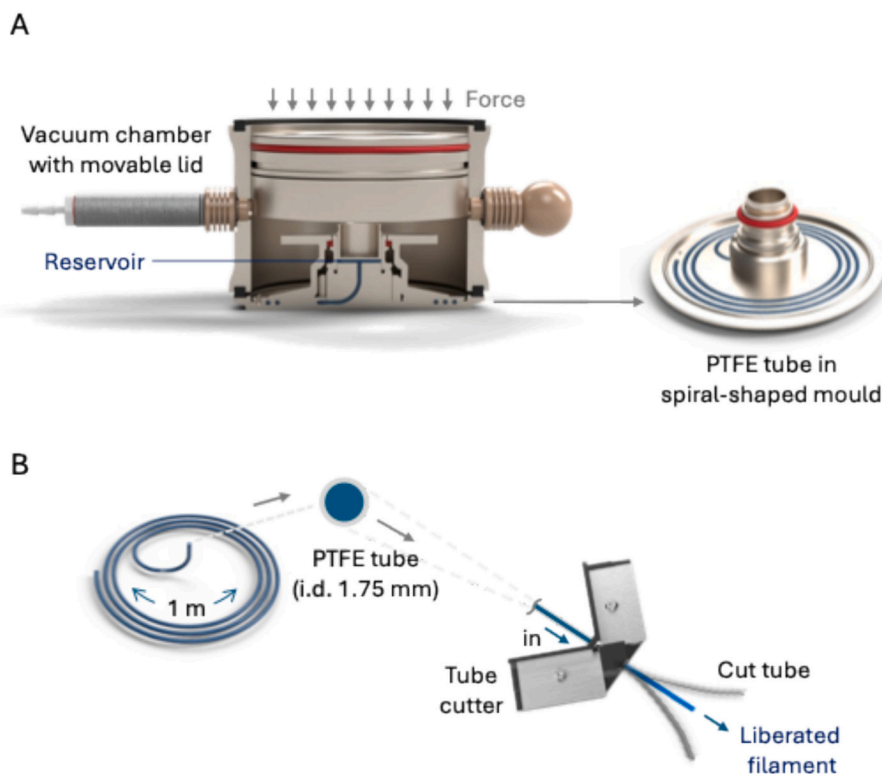
Fig. 1. Overview of working principles of VCM filament moulder channel system for filament fabrication. A) Formulation or pre-compressed VCM disc is loaded into system reservoir, which under application of vacuum pressure and heat fills a PTFE tube of 1.75 mm internal diameter fitted inside a spiral-shaped channel mould. B) Cooled filament is liberated from PTFE tube by passing through a razor blade-lined tube cutter.

Instrumentation, Southport, UK) at three separate sections.

2.2.3. 3D printing of printlets

Cylindrical printlets containing three different tamoxifen doses were printed using the manufactured pharma-ink. The printlet sizes (diameter x height) were 6.0 × 2.0 mm, 8.0 × 2.2 mm, and 9.8 × 2.2 mm. The nominal doses were 10, 20, and 30 mg tamoxifen base (from here referred to only as tamoxifen) corresponding to 15.2, 30.3, and 45.5 mg TC. Each dose group was printed from a different batch of pharma-ink.

The printlets were designed and sliced using the M3DIMAKER Studio software (v2.4.1, FABRX Artifical Intelligence, Currelos, Spain) and printed with a 0.2 mm layer height using a 0.4 mm nozzle heated to 120 °C in the FDM printhead function for the M3DIMAKER2 (FABRX, London, United Kingdom) pharmaceutical 3D printer. The printlets consisted of two shell perimeters and 100 % infill in a rectilinear pattern. The printing speeds were: 15 mm/s for perimeters, 20 mm/s for infill with 15 mm/s infill for top layer. The first layer was printed at 15 mm/s, and the speed of travel was 60 mm/s.

2.2.4. Uniformity of mass and dimensionality

Masses and dimensions were measured for each printed dose ($n = 10$) using an analytical balance and a digital Vernier calliper (GNW Instrumentation, Southport, UK). The acceptance value (AV) for the uniformity of mass for printlets of each dose was calculated according to Table 2.9.40.-2 in Ph. Eur. chapter 2.9.40, using Eq. (1)

$$AV = |M - \overline{X}| + ks \qquad (1)$$

where $M = \overline{X}$ if $98.5\% \leq \overline{X} \leq 101.5\%$, $M = 98.5\%$ if $\overline{X} < 98.5\%$, $M = 101.5\%$ if $\overline{X} > 101.5\%$, $k = 2.4$, and $s = \left[\frac{\sum_{i=1}^{n}(x_i - \overline{X})^2}{n-1} \right]^{\frac{1}{2}}$. Mass variations were within specified limits if calculated AVs were below 15.0.

Table 2
Compositions of VCM calibration formulations used for NIR quantitative model.

Formulation	TC (% w/w)	Klucel ELF (% w/w)	Mannitol (% w/w)	Polyplasdone-XL (% w/w)	MgSt (% w/w)
20 % TC	20	42.7	16.0	16.0	5.3
22 % TC	22	41.6	15.6	15.6	5.2
24 % TC	24	40.5	15.2	15.2	5.1
26 % TC	26	39.5	14.8	14.8	4.9
28 % TC	28	38.4	14.4	14.4	4.8
30 % TC	30	37.3	14.0	14.0	4.7

2.2.5. Uniformity of content and dose

The tamoxifen content for each printlet size ($n = 10$) was assessed by placing each individual printlet in a volumetric flask (VF) which was q.s. with mobile phase (MP (see Section 2.2.7 for solvent composition)) and stirred using a magnetic stirrer overnight (400 rpm). A portion of the resulting solution was filtered through a 0.22 μm syringe filter (Merck Life Sciences, Watford, United Kingdom) before four-fold dilution with MP for a nominal tamoxifen concentration of 0.25–0.30 mg/ml and transfer to amber HPLC vials. The samples were analysed via HPLC according to Section 2.2.7. The AVs for tamoxifen content according to Ph. Eur. Chapter 2.9.40 for each dose group were calculated using Eq. (1) specified in Section 2.2.4. Content uniformity was verified if calculated AVs were below 15.0.

2.2.6. Characterisation of PM, pharma-ink, and printlets

2.2.6.1. Thermogravimetric analysis (TGA).
TGA analysis was performed using a Discovery TGA (TA Instruments-Waters LLC, New Castle, DE, USA). Raw materials (TC and excipients) with average samples sizes of 3–5 mg in open aluminium pans were heated at 10 °C/min from 30 °C to 200 °C under nitrogen purge gas at a flow rate of 25 ml/min. All raw

materials (TC, Klucel ELF, D-Mannitol, Polyplasdone-XL, MgSt) as well as the powder formulation and prepared filament were analysed for potential mass loss upon isothermal conditions at 130 °C to simulate the filament preparation process. Average sample sizes of 3–5 mg in open aluminium pans were heated at 10 °C/min from 30 °C to 130 °C and maintained at 130 °C for 30 mins under nitrogen purge gas at 25 ml/min. Data collection and analysis were completed using TA Instruments Trios software (v4.5.0.42498, TA Instruments-Waters LLC, New Castle, DE, USA).

2.2.6.2. Differential scanning calorimetry (DSC).

DSC analysis was performed using a Q2000 instrument (TA instruments-Waters LLC, New Castle, DE, USA) and TA aluminium pans sealed with pin-hole hermetic lids (Tzero). Samples of an average mass of 3–5 mg were equilibrated at 25 °C before heating to 100 °C to evaporate any adsorbed moisture. Then they were cooled to and equilibrated at 25 °C, before heating again to 160 °C. Nitrogen was used as purge gas at 50 ml/min flow rate. Data were collected using the TA Advantage software for Q series (v2.8.394, TA Instruments-Waters LLC, New Castle, DE, USA) and analysed with the TA Instruments Universal Analysis 2000. Raw materials (TC, Klucel ELF, D-Mannitol, Polyplasdone-XL, and MgSt), formulation PM, pharma-ink (filament), and printed disc (23 × 0.4 mm) were analysed.

2.2.6.3. X-ray powder diffraction (XRPD).

Raw materials for the formulation (TC, Klucel ELF, D-Mannitol, Polyplasdone-XL, and MgSt) as well as the PM and printed disc (23 × 0.4 mm) of the formulation were analysed for their XRPD patterns. A Rigaku MiniFlex 600 (Rigaku, Tokyo, Japan) equipped with a Cu Kα X-ray source ($\lambda = 1.5418$ Å) was utilised with the application of 40 kV voltage and 15 mA current. Samples were scanned between 3 and 40° 2θ with a step size of 0.02° and a speed of 5°/min.

2.2.6.4. Fourier transform infrared spectroscopy (FT-IR).

FT-IR spectra were collected using a Spectrum 100 FTIR spectrometer (PerkinElmer, Waltham, MA, USA). Spectra were collected for all samples over the range 4000–650 cm^{-1} with a resolution of 4 cm^{-1} for 16 scans. Raw materials (TC, Klucel ELF, D-Mannitol, Polyplasdone-XL, and MgSt), PM and printed disc (23 × 0.4 mm) were analysed.

2.2.6.5. Scanning electron microscopy (SEM).

SEM images of the curved printlet sides were acquired for the 20 mg printlets to assess the layer deposition and fusion. A Phenom Pro (Phenom-World BV, Eindhoven, Netherland) with an acceleration voltage of 15 kV was utilised for high-magnification image acquisition. The printlet was cut in half along the vertical axis using a scalpel, and the cross-section was attached to a self-adhesive carbon disc placed on a 25 mm aluminium stub. The sample was gold coated for 60 s using a rotary coater (Q150R S Plus, Quorum, United Kingdom).

For lower magnification images, the printlet was placed whole on a self-adhesive carbon disc mounted onto a 25 mm aluminium stub and the sample was sputter coated with 25 nm gold. The stub was placed in a Quanta 200 FEG SEM (FEI, Altrincham, United Kingdom) and analysed using 5 kV accelerating voltage.

2.2.6.6. X-ray micro-computed tomography (micro-CT).

X-ray micro-computed tomography (micro-CT) analysis was performed on one printlet per size and a fragment of the pharma-ink (ca. 1 cm in length cut with a scalpel) using a SkyScan1172 (Bruker, Kontich, Belgium). Image acquisition settings were 55 kV source voltage and 171 µA source current. The image resolution was 4000 × 2096 pixels with each image pixel being 3.54 µm (10 mg printlet), 5.14 µm (20 mg printlet), 5.90 µm (30 mg printlet), and 3.37 µm (pharma-ink). The object was rotated 360° at a rotation step of 0.15° with a two-frame average per step. Image reconstruction was carried out with NRecon software (version 1.7.5.4, Bruker, Kontich, Belgium) and 3D volume rendering was done with

CTvox software (version 3.2.0 r1294, Bruker, Kontich, Belgium) where each pixel in the 3D rendered object was colour mapped according to X-ray density. 3D printlet models were generated with CTan software (version 1.16.4.1, Bruker, Kontich, Belgium) then cleaned and processed using Python (version 3.11.7) with libraries numpy-stl (version 3.1.1) and trimesh (version 4.4.3) and the open-source software MeshLab (ISTI-CNR, Pisa, Italy) to extract the bounding box dimensions along the x and y axes to confirm equal aspect ratios.

2.2.6.7. Tamoxifen solubility and in vitro dissolution testing.

TC solubility in 0.02 N HCl with and without Klucel ELF at 37 °C was assessed to ensure that sink conditions would be maintained throughout the in vitro dissolution testing and to investigate if Klucel ELF could enhance TC solubility. Excess TC was added to a vial with 5 ml 0.02 N HCl ($n = 3$) and 74 µg/ml Klucel ELF in 0.02 N HCl ($n = 3$). The vials were covered with foil and left to stir on a heated magnetic stirrer plate set at 37 °C (300 rpm) for 48 h. Samples were filtered through 0.22 µm syringe filters (Merck Life Sciences, Watford, United Kingdom) and immediately diluted by 10× with 0.02 N HCl for analysis by HPLC (Section 2.2.7). The mean TC solubilities were compared for difference of statistical significance by an unpaired *t*-test ($p < 0.05$) using GraphPad Prism (v10.1.0, Dotmatics, Boston, USA). The concentration of Klucel ELF was determined based on the theoretical content in the largest printlet size, hence the highest amount of TC needing solubilisation.

Printlets from each dose were subjected to in vitro dissolution testing ($n = 3$) using a 708-DS USP-I apparatus (Agilent Technologies, Stockport, United Kingdom) in 1000 ml of 0.02 N HCl (prepared by dilution of 5 M HCl) maintained at 37 ± 0.5 °C under constant basket rotation (100 rpm). 2 ml samples were withdrawn and filtered through 0.22 µm syringe filters (Merck Life Sciences, Watford, United Kingdom) into HPLC vials at 1, 2, 3, 4, and 5 h with medium replacement. The samples were analysed via HPLC as described in Section 2.2.7. Sink conditions were maintained throughout all tests.

Factors for difference ($f1$) and similarity ($f2$) between dissolution profiles from the printlets of different sizes were calculated according to U.S. Food and Drug Administration (FDA) guidelines. Calculations were based on mean drug release from timepoints of ≥15 % drug release and the first timepoint of ≥85 % drug release. Release profiles were considered similar if $f1 = 0 - 15$ and $f2 = 50 - 100$.

2.2.7. High performance liquid chromatography (HPLC)

A Hewlett Packard 1260II Series HPLC system equipped with an online degasser, quaternary pump, column heater, autosampler, and UV/Vis detector was utilised. Samples were injected at a flow rate of 1 ml/min into a Hypersil ODS C18 5 µm, 250 × 4.6 mm column (Thermo Fisher Scientific, Cheshire, United Kingdom) maintained at 30 °C. The MP was prepared by dissolving 506 mg $NaH_2PO_4 \cdot H_2O$ in 600 ml water, adding 3.76 ml DMOA, adjusting the pH to 3.0 (± 0.03) with phosphoric acid, and mixing with 490 ml ACN. Two injection volumes were applied; 10 µl for samples dissolved in MP (calibration curve range 0.033–0.66 mg/ml tamoxifen; $R^2 = 0.9999$, LoQ = 0.016 mg/ml, and LoD = 5.3 µg/ml), and 50 µl for samples dissolved in 0.02 N HCl (calibration curve range 2.5–60 µg/ml tamoxifen; $R^2 = 0.9998$, LoQ = 2.2 µg/ml, and LoD = 0.74 µg/ml). Eluents were analysed at 240 nm.

2.2.8. Quantitative NIR model development through VCM for dose verification of printlets

Calibration formulations were prepared from 20 % *w/w* to 30 % *w/w* TC in intervals of 2 % *w/w* with excipients scaled equivalently to the developed formulation consisting of 25 % *w/w* TC (Table 2). Formulations were mixed using a mortar and pestle. Approximately 130–140 mg PM from Table 2 ($n = 3$) were weighed into the VCM Disc Tool D08 (8 mm diameter) and compressed for five min under application of vacuum and 130 °C then cooled to room temperature under continued vacuum pressure using the VCM instrument (MeltPrep GmbH, Graz, Austria).

NIR diffuse reflectance spectra were recorded over the range 950–1650 nm (10,526–6060 cm^{-1}) using a MicroNIR 1700ES spectrometer (VIAVI, Newbury, United Kingdom) equipped with two vacuum tungsten lamps and an InGaAs photodiode array detector. A tablet probe with 8 mm collection optic (VIAVI, Newbury, United Kingdom) was attached to the MicroNIR instrument for spectra collection with the MicroNIR Pro software (VIAVI, Newbury, United Kingdom). The instrument was calibrated through dark and reference spectra of a 99 % spectralon reference standard (VIAVI, Newbury, United Kingdom) with recalibration every 10 min throughout sample spectra acquisition. Each sample was placed at the 99 % spectralon standard and scanned 10 times for 11 ms per scan. Scanned samples included the 6 VCM calibration concentrations ($n = 3$) and FDM printlets of the intermediate size ($n = 8$) for model evaluation and dose verification. The tamoxifen, and hence TC, content of each calibration and validation sample was determined using HPLC, as described in Section 2.2.5.

Spectral pretreatments and model development with HPLC determined TC content in calibration and validation samples were carried out using python (version 3.9.9), a function available through the M3DIMAKER studio software (v2.4.1) (FABRX, London, United Kingdom). Specific libraries used included numpy, pandas, matplotlib. pyplot, scipy, sklearn, and math. Models were evaluated on their coefficient of determination (R^2), R^2 upon 10-fold cross validation (CV) by leave-one-out method, and root mean square error of calibration (RMSEC) for the calibration data. Predictive performance was assessed by root mean square error of prediction (RMSEP) for the FDM printlets.

Tamoxifen doses in the FDM printlets were determined through the predicted TC concentration from the chemometric model and the respective printlet masses recorded off-line using an analytical balance. A paired *t*-test was performed on HPLC established tamoxifen doses and those found from the NIR model prediction for the FDM printlets using GraphPad Prism (v10.1.0, Dotmatics, Boston, USA).

3. Results and discussion

3.1. Dimensional and content uniformity of printlets

Pharma-inks containing 25 % *w/w* tamoxifen citrate of consistent diameter of 1.75 ± 0.01 mm (relative standard deviation (RSD) = 0.659 %) were successfully manufactured using the VCM filament moulder system for subsequent FDM 3DP of printlets containing three different tamoxifen base doses (Fig. 2). The printlets of the 3 different sizes displayed a high level of intra-group dimensional uniformity both in terms of resulting diameter and height, indicative of consistent pharma-ink in terms of diameter and compositions. For all three printlet sizes, the RSD was ≤0.35 % in terms of intra-group diameter and < 2 % in terms of intra-group printlet height (Table 3).

Macroscopically, the printlets were uniform and with appropriate

layer depositions. Printing with a 0.4 mm nozzle and a layer height of only 0.2 mm yielded printlets with fine layer structures as visible from SEM images presented in Fig. 3. From the SEM images, the printlet layers seem slightly irregular with the seeming presence of particulates in the fused layers. Moreover, small gaps between each deposited layer upon FDM printing were present as a consequence of the particulates when imaged through SEM, indicating that the layers may not have been completely fused together. This was likely a result of the incorporation of excipients not reaching melting temperatures during the 3D printing processes, such as mannitol and Polyplasdone-XL, which in total accounted for 30 % *w/w* of the formulation.

Pharmaceutical FDM 3DP relies on the constant feeding of pharmaink (drug-loaded thermoplastic filament) through a heated nozzle. Most FDM printers used in pharmaceutical manufacture and research requires feeding of a pharma-ink with a 1.75 mm diameter [17]. Inconsistencies in pharma-ink diameter may result in either lack of gear grip on the filament or inability of pharma-ink to be fed into the nozzle for melting and extrusion [44]. The current standard production method for FDM pharma-ink is through HME, where a powder or granulated blend is fed through a single or twin-screw system under the application of heat for extrusion through an interchangeable die size. Maintaining a consistent diameter of the FDM pharma-ink from HME can be challenging and may require bulky setups such as conveyor belt systems to remove the pharma-ink from the die at a constant rate [27,44,45]. Optimising the die size as well as extrusion and conveyor belt speeds requires extensive trial-and-error approaches and is largely dependent on the formulation composition. Especially polymers, usually the main formulation constituent enabling FDM 3DP, display different levels of die swell upon extrusion which impacts the HME processing and collection conditions [17,46]. The new VCM pharma-ink preparation technology eliminates the need for such setups. Although the current configuration only allows small-scale production, this is a very valuable setup when developing formulations as creating one pharma-ink of up to one meter was here achieved with ca. 2.5 g of PM whereas up to 10 times that amount would have been needed for a single HME trial. A high drug-loading of 25 % *w/w* was achieved here, meaning that the reduction in material required for one trial would not only significantly implicate the associated costs but also reduce the overall environmental footprint for each trial.

The resulting printlets were assessed for their mass variation (Table 3). For all 3 dose groups, a relative standard deviation (RSD) well below 2.0 % was obtained, highlighting the consistency in mass for the printlets. No guidelines specific to 3DP medicines are yet available, thus existing monographs for conventional medicines from the different pharmacopoeias tend to be applied in the evaluation of printlet quality. The calculated AV, according to Ph. Eur. Chapter 2.9.40 for oral solid dosage forms, for each dose group of printlets was lower than the maximum tolerated AV of 15.0 (Table 3). Thus, the masses of all three
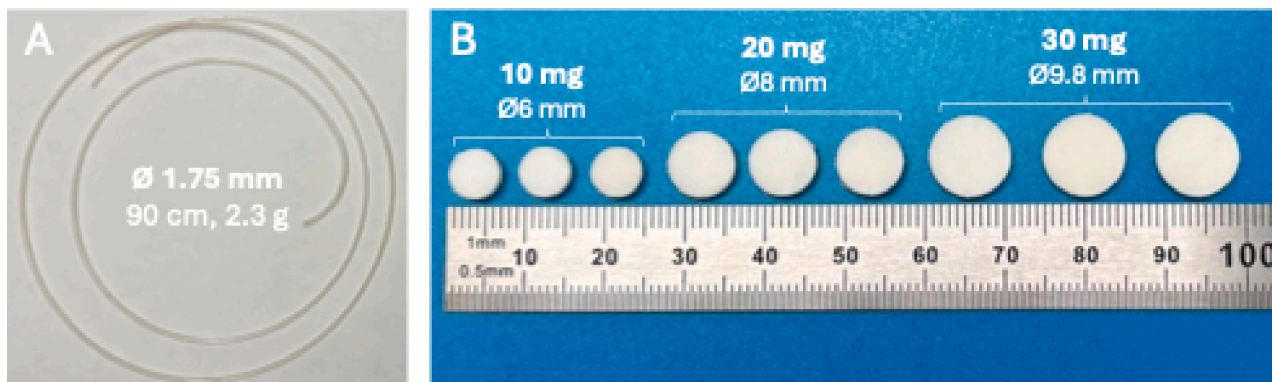

Fig. 2. A) Image of VCM produced pharma-ink (filament) containing tamoxifen and B) image of three printlets of 10 mg, 20 mg, and 30 mg tamoxifen base (left to right). Scale in mm.

Table 3

Printlet dimensions, actual tamoxifen doses, and AVs for uniformity of mass and tamoxifen content based on Ph. Eur. specifications for the printlets of 3 different sizes ($n = 10$).

Nominal dose (mg)	Diameter (mm)	Height (mm)	Mass (mg)	Mass uniformity AV	Actual dose (mg)	Content uniformity AV
10	6.24 ± 0.02	2.02 ± 0.03	61.83 ± 1.03	1.6	9.52 ± 0.31	10.8
20	8.27 ± 0.03	2.28 ± 0.03	124.6 ± 2.03	4.9	19.00 ± 0.47	9.2
30	10.08 ± 0.02	2.23 ± 0.04	183.43 ± 2.96	3.8	29.40 ± 0.67	5.9
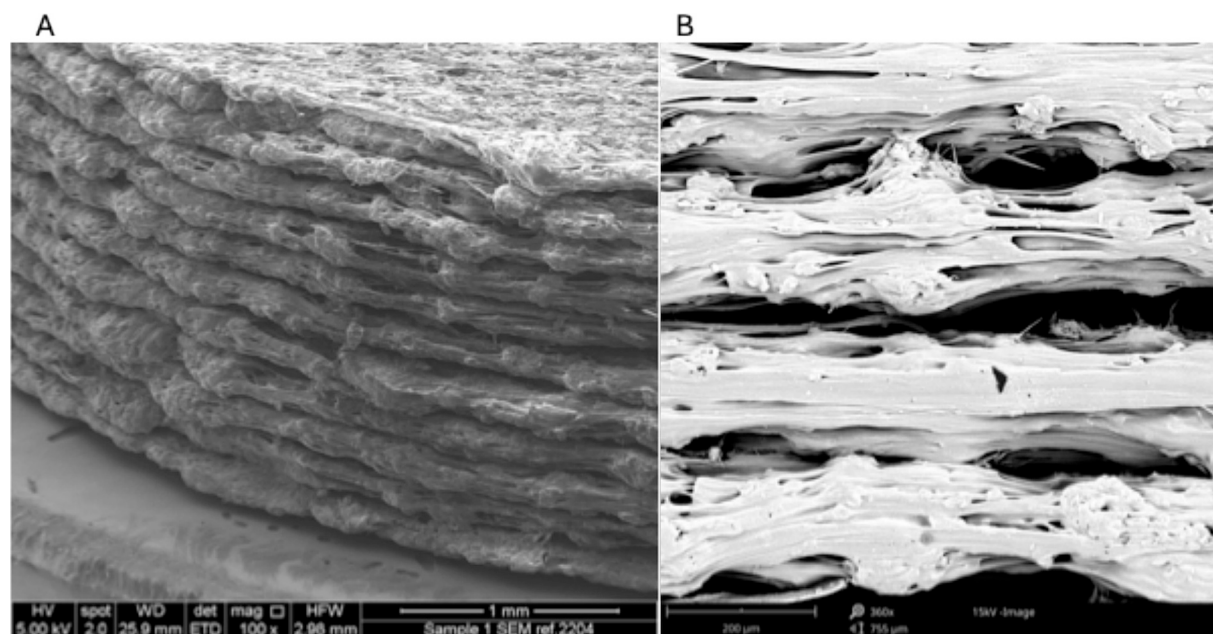
Fig. 3. SEM images of 20 mg printlets acquired with (A) Quanta 200 FEG and (B) Phenom Pro SEM instruments.

printlet sizes could be considered uniform according to Ph. Eur. specifications for mass variation.

The reconstructed and volume rendered micro-CT images revealed structural information about the printlets and filaments as well as level of uniformity in the samples. The colour mapping of the entire pharma-ink segment (Fig. 4C-D) and the cross-sectional view seemed to suggest that material of lower density had accumulated on the surface of the pharma-ink as a higher proportion of lower-density pixels were present here as compared to their distribution across the internal volume of the segment. Viewing the volume rendered printlet (Fig. 4A-B), a more uniform distribution of material was seen. Analysing the partial and angled cross-sectional cutout (Fig. 4A), some layering artifacts from the 3D printing process were visible, creating visible layering patterns in the volume rendered object. From the internal circular cutout (Fig. 4B), the layering effects were less profound and no areas of great disproportionality in terms of material distribution were visible. The bounding box dimensions (X and Y) were 6.25 and 6.03 mm for the 10 mg printlet, 8.46 and 8.29 mm for the 20 mg printlet, and 10.14 and 10.12 mm for the 30 mg printlet. This is equivalent to aspect ratios (X/Y) of 1.04, 1.02, and 1.00, respectively, thus confirming the accurate printing process of printlets of equal x and y dimensions.

The Ph. Eur. and USP apply different specifications for acceptable drug content variation within pharmaceutical dosage forms. While the Ph. Eur. applies a general monograph for mass and content uniformity for oral solid dosage forms, the USP specifies medicine-specific monographs with specific requirements. The USP monograph for conventional tamoxifen citrate tablets of 20 mg tamoxifen base specifies that the tamoxifen content must be within 90–110 % of the label claim to be accepted. The actual tamoxifen content of the claim for each of the 10 printlets per dosage group has been presented in Fig. 5. All the printlets were within the USP acceptance limits for tamoxifen content. In

addition, the calculated AVs for content uniformity were all below 15.0 based on the Ph. Eur. solid dosage form content uniformity monograph (Chapter 2.9.40) which confirmed that the tamoxifen content in all 3 printlet sizes were within the accepted range as specified by the Ph. Eur as well.

Mean tamoxifen content for the dose groups were 95.16 % (10 mg), 94.98 % (20 mg), and 97.99 % (30 mg), respectively. Unlike HME systems with single or twin-screw components, the VCM equipment does not comprise a mechanical mixing component. Thus, mixing in the VCM instrument solely relies on diffusive processes, which are inherently slow for mixing at large length scales (e.g. coarse particles of different components) but works well when length scales are small ($< \sim$50–100 µm). Therefore, a highly homogenous PM before VCM compaction and filament generation would be required to obtain pharma-ink with satisfactory material distribution. As shown in both content uniformity and micro-CT analysis, some levels of uneven material distribution may be present across the pharma-ink and printlets, however, overall dose uniformities of the printlets are within accepted ranges from both Ph. Eur. (Table 3) and USP (Fig. 5). Achieving a mean tamoxifen dose around 100 % in drug loading may be accomplished through the employment of more sophisticated mixing procedures such as milling techniques for production of the PM for the pharma-ink fabrication, however, there may be a chance that low-density materials could still create a coating-like effect.

3.2. Characterisation of raw materials, PM, and printlets

TGA analysis was performed to assess the thermal stability of all raw materials contained in the formulation. All excipients displayed thermal stability across the temperature range 30–200 °C, but tamoxifen citrate exhibited significant mass loss from ca. 150 °C (Fig. 6A). The results
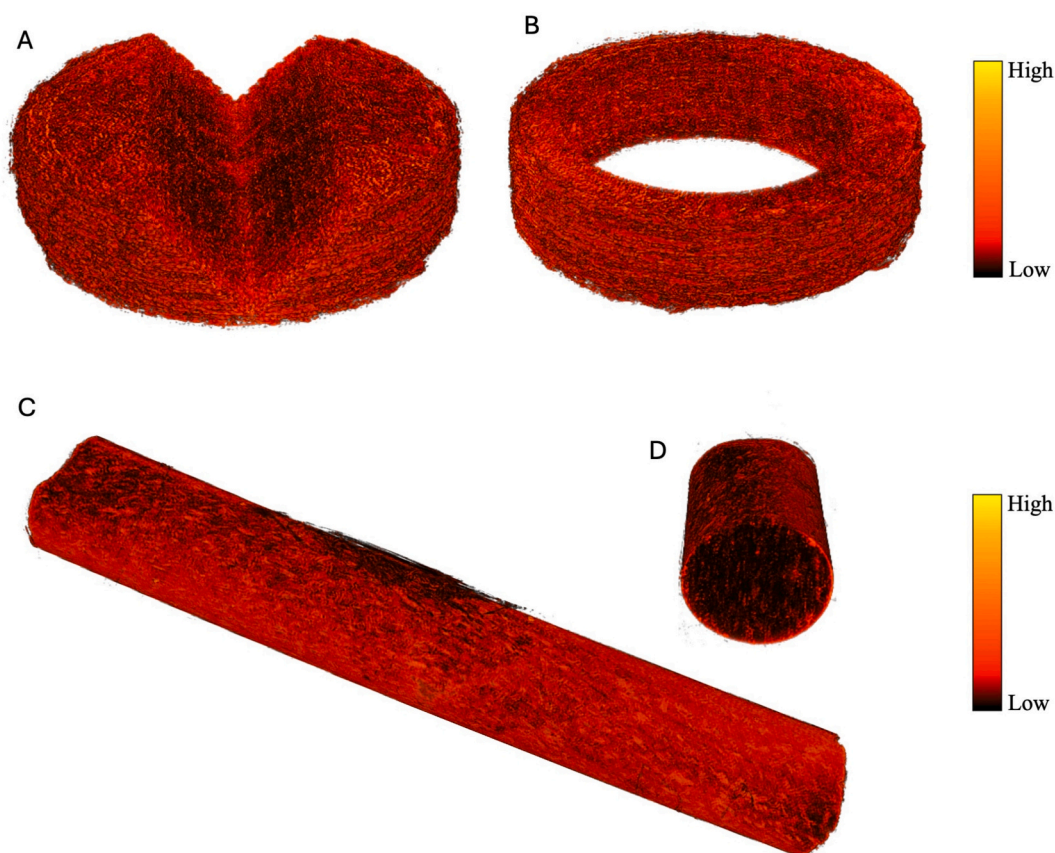
Fig. 4. Reconstructed and volume rendered micro-CT images of 20 mg printlet (A - triangular cutout along z-axis of printlet; B – cylindrical cutout along z-axis of printlet), and pharma-ink segment (C – entire segment; D – cross-section). Colour mapping denotes x-ray density of each pixel in the reconstructed images as a gradient from low to high.
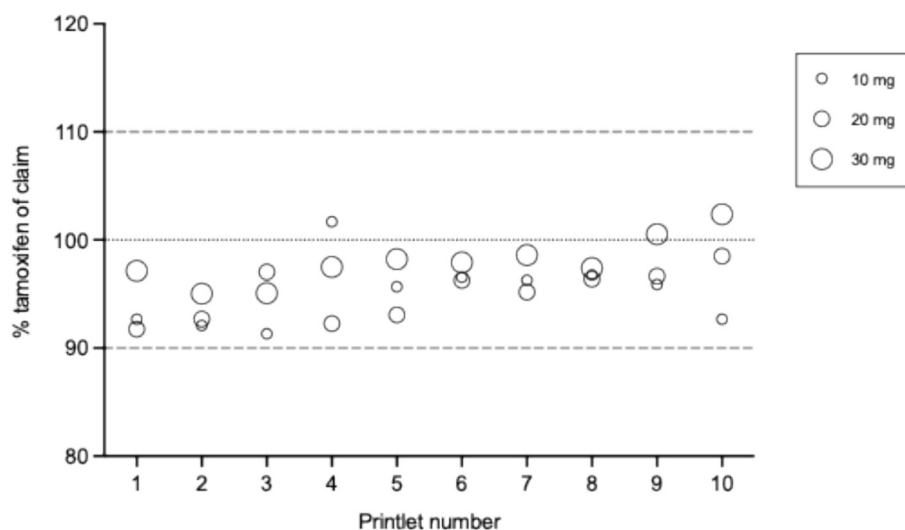

Fig. 5. Content for 10 printlets of each size, specified as percent content tamoxifen of claimed amount, i.e. 10, 20, and 30 mg tamoxifen base. Dashed lines at 90 % and 110 % indicate the acceptance limits of tamoxifen content as per the USP monograph for conventional tamoxifen tablets of 20 mg tamoxifen base.

indicated the suitability of all materials for the employed VCM processing temperature of up to 130 °C. Two excipients, namely Polyplasdone-XL and MgSt, exhibited small mass losses between temperatures of 50–100 °C, which was attributed to the evaporation of adsorbed moisture due to the hygroscopicity of these materials [47,48]. The two polymeric excipients, Klucel ELF and Polyplasdone-XL, were dried in an oven at 50 °C prior to VCM processing to ensure excipients free of as much adsorbed moisture as possible to avoid pressure disruptions during pharma-ink preparation.

In addition, isothermal TGA analysis at 130 °C for 30 min was performed on tamoxifen citrate, the formulation PM, and pharma-ink to assess if any mass loss would be observed due to prolonged exposure to the processing temperature following an initial ramp of 10 °C/min from 30 to 130 °C. A change in mass for TC of 0.2 % was observed whilst the
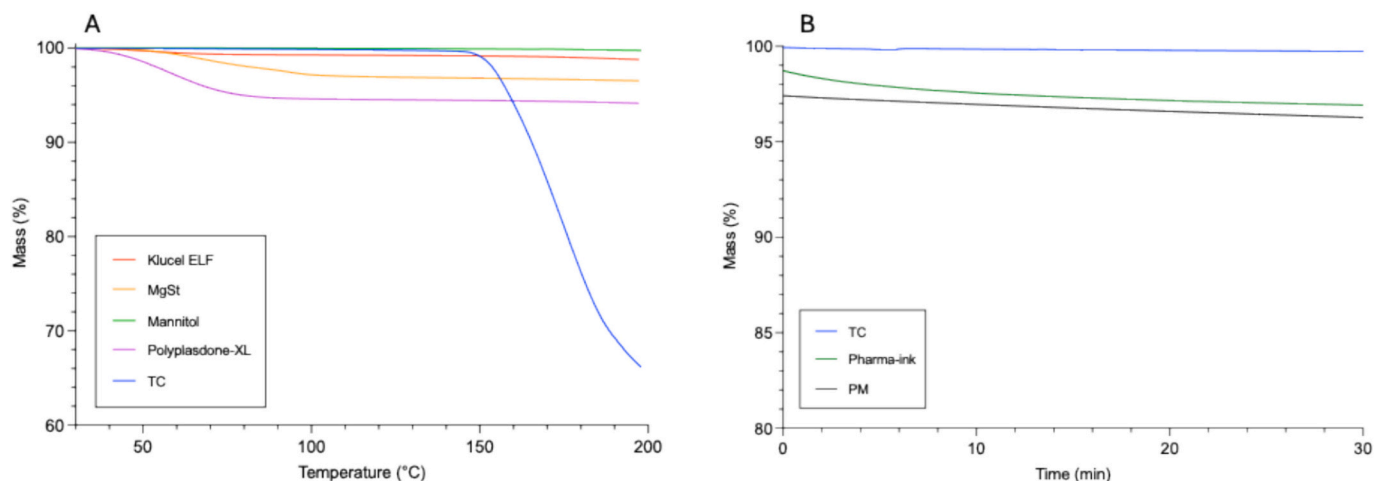
Fig. 6. A) Thermogram of mass loss of raw materials used in formulation during TGA heat ramp from 30 °C to 200 °C. B) Thermogram of mass loss of raw tamoxifen citrate, PM, and pharma-ink (filament) during isocratic heat exposure at 130 °C.

decrease was 1.1 % for PM and 1.8 % for the pharma-ink (Fig. 6B). The pharma-ink was produced by maintaining the VCM disc at 130 °C for 20 min, with the VCM disc produced from the PM at 110 °C for 5 min prior. Although the effect of vacuum was not accounted for in the analysis, the time of exposure to the temperature was increased. The pharma-ink would be exposed to 120 °C momentarily during the printing process, thus the overall mass loss seen during the isothermal analysis of the pharma-ink was expected to be exaggerated. Most of the mass loss for the PM and pharma-ink were observed during the ramp from 30 to 130 °C, likely the evaporation of adsorbed moisture, hence the lower percentage of remaining mass at the start of the isothermal analysis was observed. As such, no significant thermal tamoxifen decomposition was expected during the VCM manufacture of the pharma-ink nor printlets, concluded from the isothermal thermograms of tamoxifen citrate, PM, and pharma-ink.

Solid state analyses were performed on all raw materials as well as the PM and printlet of the formulation. Both DSC and XRPD were performed to determine any transitions in solid state of tamoxifen citrate. The DSC thermogram of tamoxifen citrate powder yielded a melting point of approximately 147.5 °C (Fig. 7). The only excipient displaying any thermal events in the investigated window was MgSt. The double endothermic peaks at ca. 112 °C and 124 °C suggest a hydrate form of MgSt which may have been formed during storage of the material

[49–51]. Two small endothermic events are present in the thermogram for the formulation PM at ca 126 °C and 139.5 °C. These may be attributed to either 1) presence and partial solubilisation of two different tamoxifen citrate polymorphic forms formed during the initial heat ramp to 100 °C and cooling cycle, or 2) partial tamoxifen or mannitol solubilisation, and altered thermic properties of MgSt after initial heat ramp to 100 °C and cooling cycle accounting for the two endotherms. Melting point depression of mannitol, which has a reported melting point of ca. 167 °C [52], was not likely to account for one of the endothermic events in the PM thermogram as seen from its intact crystallinity in the XRPD diffractograms for both the PM and printlet (Fig. 8). Klucel ELF has previously been reported capable of partially solubilising a Biopharmaceutics Classification System (BCS) Class II drug, ketoprofen, upon heat [53]. Moreover, Polyplasdone-XL has also been proven capable of solubilising a BCS Class II drug, indomethacin, during heat exposure [54]. Tamoxifen citrate is also a BCS Class II drug, hence the melting point depression may likely be from partial solubilisation within one or both these polymers. Nonetheless, no endothermic events are present in the thermogram for the printlet. Thus, the data indicates that tamoxifen citrate is being partially solubilised by the formulation during the application of heat in the DSC analysis, while prolonged heat processing from both VCM pharma-ink generation and 3DP resulted in a greater extent of solubilisation and potentially fully changed it into its
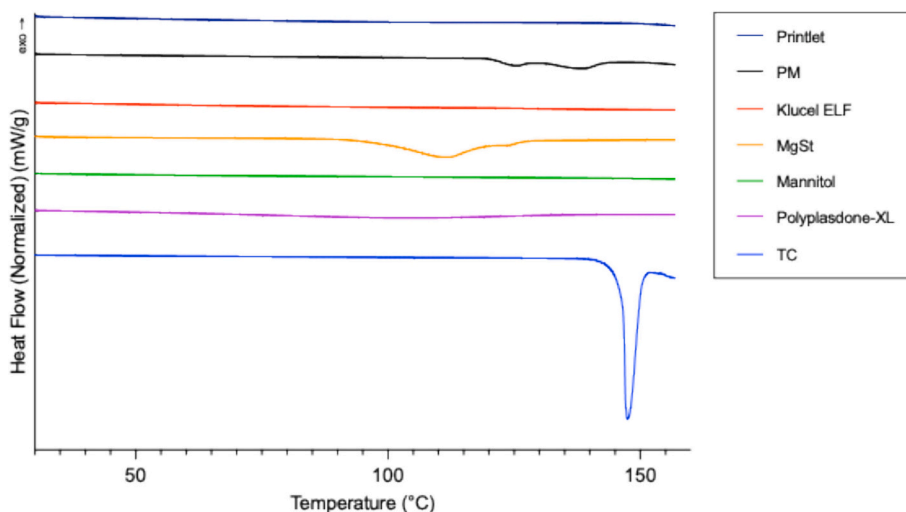
Fig. 7. DSC thermograms of second heating ramp for all raw materials used in formulation, PM and printlets.
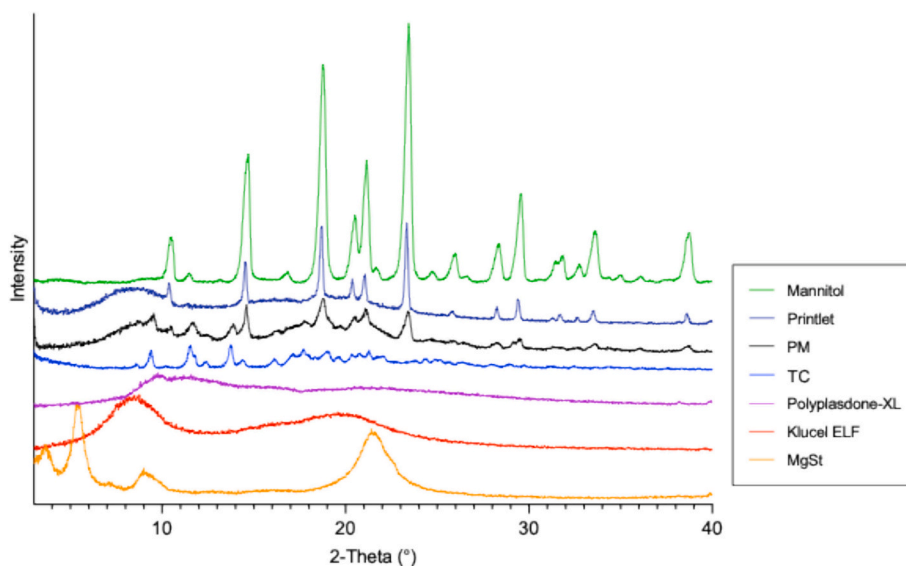
Fig. 8. XRPD diffractograms of the raw materials, PM, and printlets.

amorphous form.

The XRPD patterns obtained from of the raw materials, PM, and printlet are presented in Fig. 8. Pure tamoxifen citrate showed distinct diffraction peaks at ca. 11.5° and 13.8° 2θ, and the shape and intensities of these diffraction peaks alongside the absence of a distinct diffraction peak at ca. 5.5° 2θ confirm the presence of the polymorphic form A, as previously reported [55]. The two polymers, Klucel ELF, a semi-crystalline hydroxypropyl cellulose (HPC), and Polyplasdone-XL, a crospovidone, showed no long-range order diffraction. Mannitol exhibited a high degree of crystallinity with sharp and distinct diffractive peaks across the range 10–40° 2θ. TC diffraction peaks were present in the diffractogram for the PM, however, they disappeared in the diffractogram for the printlets with only mannitol diffractive peaks remaining. This, along with the DSC thermograms, indicated that tamoxifen became amorphously dispersed in the formulation due to the heat processing of the pharma-ink preparation and 3D printing.

The FT-IR spectra confirm tamoxifen citrate being in it its polymorphic Form A in the raw material (Fig. 9), based on the characteristic

sharp and symmetric acid carbonyl stretch at 1729 cm^{-1}, a broad asymmetric and sharp symmetric COO- stretches present at 1587 cm^{-1} and 1378 cm^{-1}, respectively [56]. Moreover, aromatic ring stretches at 1241 cm^{-1}, 1217 cm^{-1}, and para- and mono-substituted bands at 779 cm^{-1}, 767 cm^{-1}, and 703 cm^{-1}, along with a single covalent carbon-oxygen bond stretch at 1173 cm^{-1} confirm the presence of TC Form A [56]. To interpret whether any chemical changes was happening to tamoxifen citrate during the manufacturing process, the characteristic FT-IR stretches in the region 1800–700 cm^{-1} were examined as the FT-IR transmittance peaks from the -OH group around 3000–2500 cm^{-1} were likely to be masked by overlapping peaks from the excipients.

Both HPC and Polyplasdone-XL are non-ionic polymers, meaning that no polymer-drug ion complexes should form during the manufacturing process between these and tamoxifen [57]. The strong carbonyl vibration at 1729 cm^{-1}, arising from the citric acid molecules in tamoxifen citrate, remained in the spectrum for the PM but broadened in the spectrum acquired from the printlet (Fig. 9). This could indicate an interaction such as hydrogen bonding, or potentially esterification
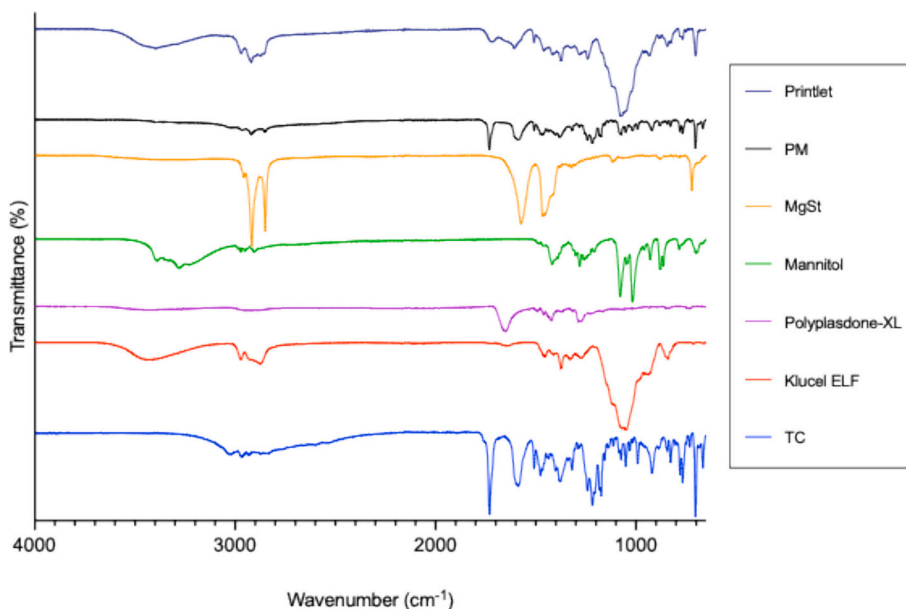

Fig. 9. FT-IR spectra of the raw materials, PM, and printlets.

[58] with mannitol, or be a consequence of tamoxifen citrate partially solubilising in the printlet matrix during heat processing. The aromatic vibrations at 1507 cm^{-1} and 1241 cm^{-1} were still present in the spectra for the PM and printlet, along with the di- and mono-substituted aromatic ring bands at 779 cm^{-1}, 767 cm^{-1}, and 703 cm^{-1}, indicating that no chemical alterations were occurring to the tamoxifen base.

The drug dissolution profiles from each printed size were investigated in 0.02 N HCl (Fig. 10). The 20 mg and 30 mg printlets showed nearly identical tamoxifen release. For 1 of the 10 mg printlets, tamoxifen release at 1 h was below the limit of quantification. Thus, this replicate accounted for 0 % tamoxifen release at this time point resulting in large error bars, although the actual release for this replicate was likely somewhere around 15 %. The 10 mg printlets displayed slightly faster tamoxifen release at every timepoint from 2 h onwards compared to the 20 mg and 30 mg printlets. This was a consequence of the larger surface area to volume (SA/V) ratio for this dose (SA/V$_{10 mg}$ = 1.67 mm^{-1}) compared to the two other doses (SA/V$_{20 mg}$ = 1.41 mm^{-1} and SA/V$_{30 mg}$ = 1.32 mm^{-1}) [45]. Nonetheless, the difference (*f1*) and similarity (*f2*) scores indicated that the dissolution profiles were similar between each dose group, as the difference scores were all below 15 whilst the similarity scores were all above 50 (Table 4). Highest similarity was found between the 20 mg and 30 mg printlets, likely due to their more closely related SA/V ratios.

For HPC polymers, the general dissolution mechanisms are through swelling and erosion. A decrease in polymer molecular weight generally results in a faster dissolution process through more rapid erosion. Klucel ELF is the Klucel HPC polymer of lowest molecular weight and should thus offer the fastest drug release from this polymer family. A recent study proved that dispersion of tamoxifen citrate in polyethylene glycol (PEG) 4000 contained in a gelatine capsule filled via a novel 3DP compounding platform resulted in complete tamoxifen release within 60 min in 0.02 N HCl [59], likely a result of the low molecular weight, and high polarity and aqueous solubility of the PEG polymer [60].

HME and VCM processing result in densely packed extrudates due to the melting and mixing of the thermoplastic polymers with APIs and/or other excipients. Moreover, this effect is maintained through FDM printing, another extrusion-based technique, where the pharma-ink is deposited layer by layer to create the desired printlet size and shape. For enhanced resolution and mechanical strength, printing of as densely packed a printlet as possible is often desired, i.e. through thin layers deposited on top of the previous layers with no or minimal inter-layer voids. The densification of the resulting printlets (arising both from the pharma-ink preparation and FDM printing process) was likely to have had implications for the resulting dissolution profiles even though
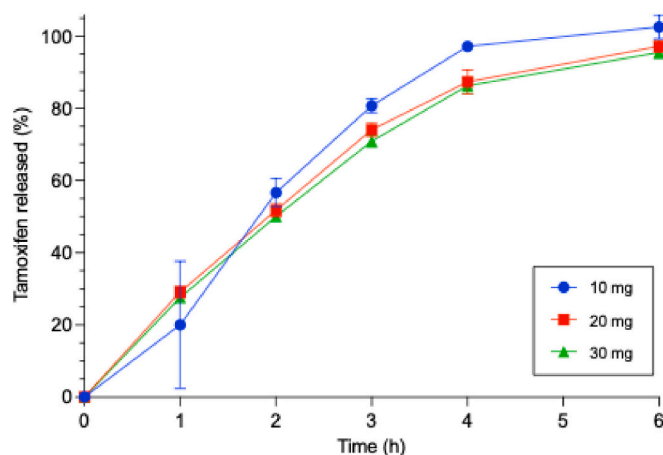

Fig. 10. Dissolution profiles of printlets containing 10 (blue circles), 20 (red squares), and 30 mg (green triangles) tamoxifen (*n* = 3) in 0.02 N HCl. (For interpretation of the references to colour in this figure legend, the reader is referred to the web version of this article.)

Table 4
Difference (*f1*) and similarity (*f2*) scores between the dissolution profiles from the different printlet sizes.

	Difference score (*f1*)	Similarity score (*f2*)
10 mg vs 20 mg	12.6	55.1
20 mg vs 30 mg	3.9	81.1
10 mg vs 30 mg	13.7	52.5

a disintegrant was included. The inclusion of crospovidone disintegrants in HME products may exert different effects when compared to inclusion in conventionally compressed tablets. Moreover, as tamoxifen was dispersed in the printlet matrix, the release of tamoxifen was dependent on the erosion of the printlet matrix, hence why the full release of tamoxifen was observed between 4 and 6 h in 0.02 N HCl for all three printlet sizes. Tamoxifen citrate has a reported solubility in 0.02 N HCl at 37 °C of app. 0.2 mg/ml [61]. Here, the solubility in 0.02 N HCl at 37 °C was found to be 0.148 ± 0.014 mg/ml whereas it was significantly enhanced to 0.219 ± 0.007 mg/ml by the presence of Klucel ELF in a concentration equal to that in the dissolution assay for the 30 mg printlet (*p* = 0.0014). Thus, the solubilising capacity of the dissolution medium was at least 4.8 times greater than any printlet dose, ensuring sink conditions for all three sizes throughout the test.

Densification of HME processed tablets containing ketoprofen, a BCS Class II drug, and Klucel ELF has previously been reported [53]. Here, the authors found that complete release of ketoprofen was achieved within 1.5 to 2 h from 1 mm pellets produced from HME. The pellet formulation consisted of Klucel ELF, Ketoprofen, and mannitol. Milling and tableting of the pellets with addition of disintegrants resulted in faster release of ketoprofen. The density of the HME pellets compared to the tablets along with the exposed surface area as a function of disintegration were the major reasons for the observed dissolution profiles. In addition, loratadine printlets, another BCS Class II compound, containing Klucel EF and Polyplasdone-XL among other excipients, printed with low infill levels of 40–60 % displayed more accelerated release due to the highly enhanced SA/V [62]. In the current study, the printlets were produced with 100 % infill and 0.2 mm thin layers, and although the formulation contained Klucel ELF, mannitol, and Polyplasdone-XL, the manufacturing process resulted in printlet densification and reduced SA/V ratio as compared to the pellets, compressed tablets, and low-infill printlets in aforementioned studies.

### 3.3. NIR model through VCM for dose determination in printlets

Determining the dose of pharmaceuticals is considered a critical quality attribute to ensure patient safety and efficacy. Since 3DP for personalised medicine has largely focused on small-scale manufacturing, it is imperative to employ adequate non-destructive methods for assuring the dose of each individual printlet as statistically based methods employed for large-scale manufacturing are infeasible. NIR spectroscopy has previously been reported as a suitable technology for API quantification in printlets produced via different 3DP technologies [39,40,63,64].

The use of NIR as a non-destructive method for determining the concentration of API requires the development of calibration models through, usually, multivariate techniques. Differentiating the concentration of API in the calibration samples is important to establish the relationship between spectral response and quality attribute. However, varying the levels of API and excipients may impact the extrudability and printability of the resulting formulations, potentially hindering the possibility to 3DP printlets of different API concentrations through a similar method, i.e. maintaining similar printing temperature. In addition, manufacturing the pharma-ink (drug loaded filaments) and producing the printlets for model calibration is time-consuming and material demanding. Therefore, this study sought to investigate whether the use of a VCM device capable of producing cylindrically shaped

objects, similar in shape to the FDM printlets produced in this study and ones generally reported, could act as calibration surrogates for determining the TC concentration in the printlets produced via FDM 3DP through the VCM manufactured pharma-ink.

The raw NIR spectra collected for all samples, including VCM calibration and 3DP validation samples, were subjected to identical spectral pre-treatment prior to model development. The raw and pre-processed spectra for one sample per sample group are presented in Fig. 11. Both additive and multiplicative scattering effects were present in the raw NIR spectra, however, application of the pre-processing notably reduced the effects of scattering between the spectra. The spectral pre-processing consisted of standard normal variate (SNV) followed by detrending with a breakpoint at the 20th spectral point before smoothing and 2nd derivation through Savitzky-Golay filter (filter width (w) of 39 and 2nd order polynomial) to remove additive and multiplicative scatter effects [65]. Where SNV reduces scatter through normalisation of the spectra, detrending fits and subtracts a linear polynomial to the drifting baseline signal often observed at higher wavelengths of solids [66,67].

The PLSR model was developed with 4 latent variables (LVs) and displayed a high coefficient of determination (R^2) of 0.997 which was maintained even upon a 10-fold cross validation (CV) by leave-one-out method (R^2 = 0.996), indicating a very robust calibration model (Fig. 12). The calibration error (RMSEC) was only 0.189 % *w/w* and the prediction error (RMSEP) was just 0.200 % *w/w* when predicting the TC
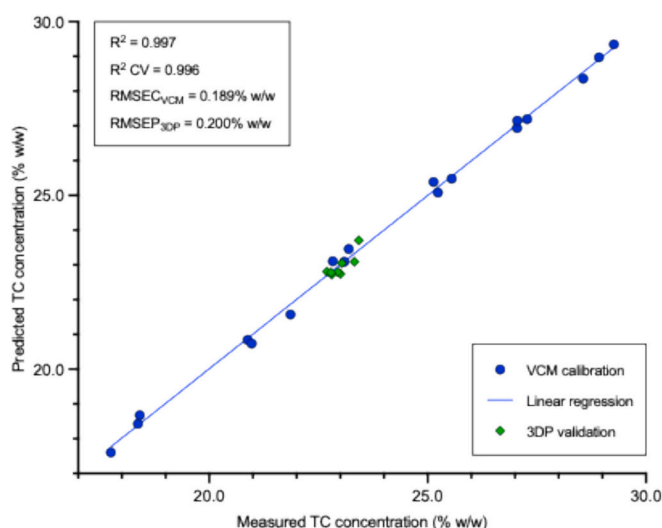
Fig. 12. PLSR model with 4 LVs developed with 8 mm diameter VCM cylindrical objects for calibration (blue circles and regression line) and validation (green rhombi) for the prediction of TC concentration in the FDM printlets. (For interpretation of the references to colour in this figure legend, the reader is referred to the web version of this article.)
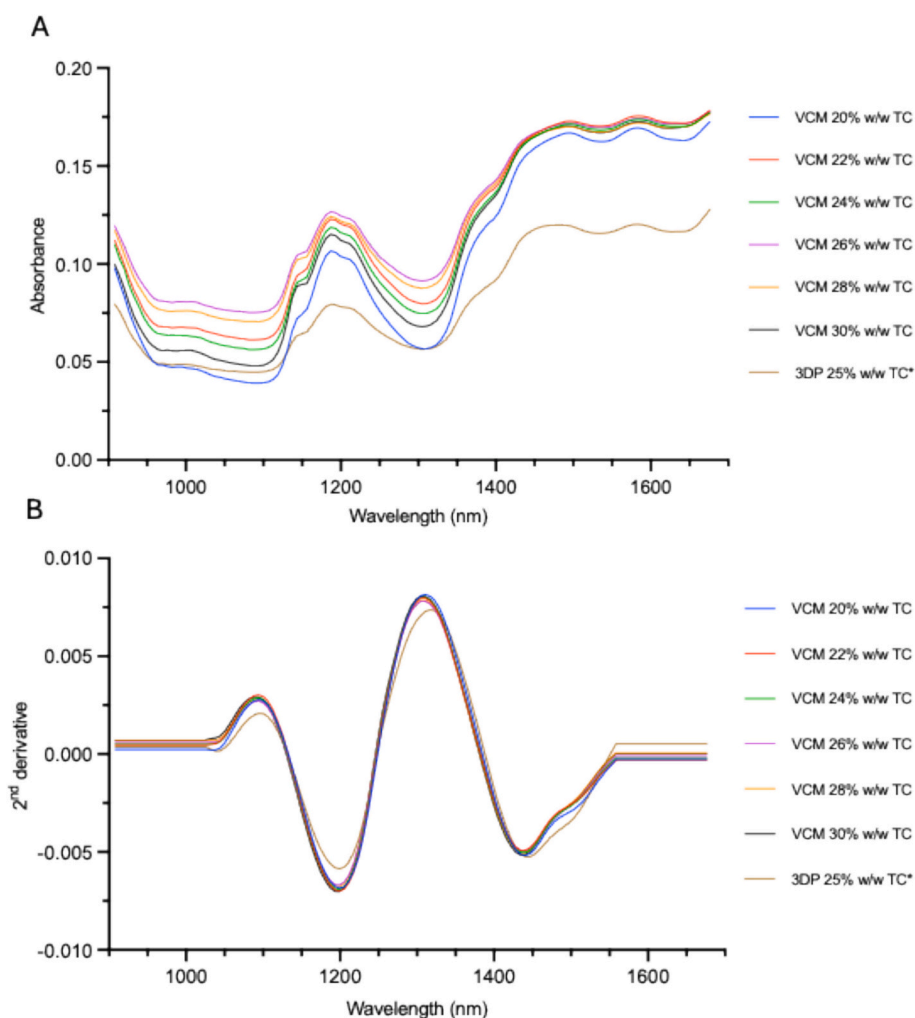
Fig. 11. Raw (A) and pre-processed (B) NIR spectra for one scan per sample group for VCM calibration and 3DP printlet validation samples. Pre-processing consisted of SNV and detrend with breakpoint at 20th spectral point and SG smoothing (w = 39, p = 2) with 2nd derivative. * Indicates 3DP validation sample.

concentration in the FDM printlets. Nearly all VCM calibration and FDM printlet samples had slightly lower TC concentrations than the nominal ones. This could be due to either loss of TC in the mixing and/or PM transfer process to VCM instrument.

Developing quantitative NIR calibration models yields the prediction of a concentration, i.e. tamoxifen citrate concentration in the VCM objects and printlets in this study. To determine the actual tamoxifen base dose, the mass of the VCM object or printlet must be known. In this study, the masses of both VCM objects and printlets were recorded offline. A recent study has reported the integration of an analytical balance into a pharmaceutical 3D printer [68], and through the use of a miniaturised NIR spectrometer, as in this study, potential integration for this may also be feasible to enable future dose predictions completely in-line of the 3DP process.

The mean predicted tamoxifen base dose in the printlets from the NIR model was 18.74 ± 0.42 mg whilst the mean dose was 18.87 ± 0.43 mg when established by HPLC. The paired *t*-test confirmed that there was no statistical difference in dose of tamoxifen base predicted from the NIR model developed on VCM surrogate samples as compared to those established by the HPLC reference method for the FDM printlets ($p = 0.5276$). This demonstrated the feasibility and suitability of non-destructively verifying the dose of tamoxifen in FDM printlets through an NIR model calibrated with VCM objects. Not only may this approach enable non-destructive dose determination for FDM printlets with less variations in processability and printability due to composition variations of the calibration formulations, it could also result in workflows necessitating the use of less material overall. Hence, a decrease in environmental footprint may be accomplished as well as costs associated with materials and resources.

NIR has previously been reported capable of accurately predicting API concentration in FDM printlets through a model calibrated with FDM printlets. A group of researchers demonstrated that caffeine content in complete FDM printlets could be accurately quantified through a handheld NIR device ($R^2 = 0.985$, RMSEC $= 0.83$ % *w/w*, RMSEP $= 1.4$ % *w/w*) across a calibration range of 0–40 % *w/w* caffeine [42]. Separately, another study reported the accurate quantitation of hydrocortisone in FDM printlets through a similar handheld NIR device across a range of 0–15 % *w/w* hydrocortisone ($R^2 = 0.981$, RMSEC $= 0.47$ % *w/w*) [39]. The surrogate NIR model developed with VCM objects in this study may therefore be considered comparable to the quantitative NIR models previously developed and calibrated with FDM printlets.

This proof-of-concept study proves that developing a surrogate NIR prediction model from VCM objects can accurately predict the tamoxifen drug concentration in printlets produced via FDM 3DP. The non-destructive NIR model developed with VCM objects would result in an overall faster chemometric NIR model development process as compared to preparing a pharma-ink and printlets per tamoxifen citrate concentration. In addition, the environmental footprint might also be slightly reduced, as minimal to no waste would be generated compared to producing excess pharma-ink for 3DP of each calibration and validation group.

4. Conclusion

FDM pharma-ink of consistent diameter (1.75 ± 0.01 mm) containing 25 % *w/w* tamoxifen citrate was successfully produced via the novel VCM filament moulding technology. Repeated pharma-ink batches were successfully produced for FDM printing of printlets containing 10 mg, 20 mg, and 30 mg tamoxifen. All printlets displayed a high level of dimensional uniformity and conformed to mass and drug content variation specifications from Ph. Eur. and USP monographs. DSC and XRPD analyses confirmed that tamoxifen was present in its amorphous form in the printlets, likely a consequence of solubilisation in the polymeric matrix as the tamoxifen citrate melting point was not reached at any point in the process. The drug release profiles between the different printlet sizes could be considered equal according to FDA guidelines. A

highly accurate NIR model for tamoxifen quantification in the FDM printlets was obtained through model calibration with cylindrical VCM objects. The model displayed excellent linearity and robustness ($R^2 = 0.997$ and R^2 CV $= 0.996$) with a low error of calibration (RMSEC $= 0.189$ % *w/w*). Moreover, a low error of prediction for the FDM produced printlets (RMSEP $= 0.200$ % *w/w*) was found with no statistical differences for tamoxifen base doses determined via HPLC and the surrogate NIR model for the FDM printlets. This study proves the synergistic effect of VCM technology for both simple and consistent FDM pharma-ink production as well as a means to develop non-destructive NIR models on surrogate samples for dose prediction of tamoxifen in FDM printlets in a rapid and easy manner with less material requirements.

CRediT authorship contribution statement

Anna Kirstine Jørgensen: Writing – review & editing, Writing – original draft, Visualization, Methodology, Investigation, Formal analysis, Data curation, Conceptualization. **Ye Chan Oh:** Methodology, Formal analysis, Data curation. **Hanxiang Li:** Data curation, Formal analysis, Methodology. **Daniel Treffer:** Writing – review & editing, Visualization, Resources, Investigation. **Maryam Parhizkar:** Writing – review & editing, Supervision, Formal analysis. **Alvaro Goyanes:** Writing – review & editing, Supervision, Resources, Project administration. **Abdul W. Basit:** Writing – review & editing, Supervision, Resources, Project administration.

Declaration of competing interest

The authors declare that they have no known competing financial interests or personal relationships that could have appeared to influence the work reported in this paper. Abdul W. Basit and Alvaro Goyanes are founders of the pharmaceutical company FABRX Ltd. and report relationships with FABRX that include equity or stocks. Daniel Treffer is the founder of company MeltPrep GmbH and reports relationship with MeltPrep that include equity or stocks. The companies had no role in the data generation, writing of the manuscript, or decision to publish.

Acknowledgements

Data availability

Data will be available upon reasonable request.

References

[1] A. Awad, E. Hollis, et al., 3D printed multi-drug-loaded suppositories for acute severe ulcerative colitis, Int. J. Pharm. X 5 (2023) 100165.

[2] V.R. Levine, M. Paulsson, et al., Off-the-shelf medication transformed: custom-dosed metoprolol tartrate tablets via semisolid extrusion additive manufacturing and the perception of this technique in a hospital context, Int. J. Pharm. X 8 (2024) 100277.

[3] H. Patel, V. Raje, et al., Application of 3D printing technology for the development of dose adjustable geriatric and pediatric formulation of celecoxib, Int. J. Pharm. 655 (2024) 123941.

[4] T. Cerveto, L. Denis, et al., The promising role of semi-solid extrusion technology in custom drug formulation for pediatric medicine, IJB 10 (6) (2024) 4063.

[5] S. Cailleaux, N.M. Sanchez-Ballester, et al., Fused deposition modeling (FDM), the new asset for the production of tailored medicines, J. Control. Release 330 (2021) 821–841.

[6] M. Rosch, T. Gutowski, et al., Development of an immediate release excipient composition for 3D printing via direct powder extrusion in a hospital, Int. J. Pharm. 643 (2023) 123218.

[7] A. Goyanes, N. Allahham, et al., Direct powder extrusion 3D printing: fabrication of drug products using a novel single-step process, Int. J. Pharm. 567 (2019) 118471.

[8] A. Awad, A. Goyanes, et al., A review of state-of-the-art on enabling additive manufacturing processes for precision medicine, J. Manuf. Sci. Eng. 145 (1) (2022).

[9] I. Seoane-Viaño, P. Januskaite, et al., Semi-solid extrusion 3D printing in drug delivery and biomedicine: personalised solutions for healthcare challenges, J. Control. Release 332 (2021) 367–389.

[10] A. Goyanes, C.M. Madla, et al., Automated therapy preparation of isoleucine formulations using 3D printing for the treatment of MSUD: first single-centre, prospective, crossover study in patients, Int. J. Pharm. 567 (2019) 118497.

[11] L. Liu, K. Fu, et al., Improving the quality and clinical efficacy of subdivided levothyroxine sodium tablets by 3D printing technology, J. Drug Deliv. Sci. Technol. 89 (2023) 105008.

[12] M. Lyousoufi, I. Lafeber, et al., Development and bioequivalence of 3D-printed medication at the point-of-care: bridging the gap toward personalized medicine, Clin. Pharmacol. Ther. (St. Louis, MO, U. S.) 113 (5) (2023) 1125–1131.

[13] L. Rodríguez-Pombo, M.J. de Castro-López, et al., Paediatric clinical study of 3D printed personalised medicines for rare metabolic disorders, Int. J. Pharm. 657 (2024) 124140.

[14] L. Rodríguez-Pombo, C. Gallego-Fernández, et al., 3D printed personalized therapies for pediatric patients affected by adrenal insufficiency, Expert Opin. Drug Deliv. (2024) 1–17.

[15] A. Goyanes, A.B.M. Buanz, et al., Fused-filament 3D printing (3DP) for fabrication of tablets, Int. J. Pharm. 476 (1) (2014) 88–92.

[16] T. Tagami, E. Kuwata, et al., Drug incorporation into polymer filament using simple soaking method for tablet preparation using fused deposition modeling, Biol. Pharm. Bull. 42 (10) (2019) 1753–1760.

[17] S. Bandari, D. Nyavanandi, et al., Coupling hot melt extrusion and fused deposition modeling: critical properties for successful performance, Adv. Drug Deliv. Rev. 172 (2021) 52–63.

[18] J. Quodbach, M. Bogdahn, et al., Quality of FDM 3D printed medicines for pediatrics: considerations for formulation development, filament extrusion, printing process and printer design, Ther. Innov. Regul. Sci. 56 (6) (2022) 910–928.

[19] S. Oladeji, V. Mohylyuk, et al., 3D printing of pharmaceutical oral solid dosage forms by fused deposition: the enhancement of printability using plasticised HPMCAS, Int. J. Pharm. 616 (2022) 121553.

[20] M. Tidau, J.H. Finke, Dispersion state analysis in hot melt extruded, highly drug-loaded 3D printing filaments applying Raman microscopy, RPS Pharm. Pharmacol. Rep. 3 (2) (2024) rqae007.

[21] H. Ponsar, R. Wiedey, et al., Hot-melt extrusion process fluctuations and their impact on critical quality attributes of filaments and 3D-printed dosage forms, Pharmaceutics 12 (6) (2020).

[22] A. Goyanes, A. Fernández-Ferreiro, et al., PET/CT imaging of 3D printed devices in the gastrointestinal tract of rodents, Int. J. Pharm. 536 (1) (2018) 158–164.

[23] J.J. Ong, B.M. Castro, et al., Accelerating 3D printing of pharmaceutical products using machine learning, Int. J. Pharm. X 4 (2022) 100120.

[24] B. Brandl, S. Eder, et al., An alternative filament fabrication method as the basis for 3D-printing personalized implants from elastic ethylene vinyl acetate copolymer, Sci. Rep. 14 (1) (2024) 2773.

[25] G. Shadambikar, T. Kipping, et al., Vacuum compression molding as a screening tool to investigate carrier suitability for hot-melt extrusion formulations, Pharmaceutics 12 (11) (2020).

[26] G. Dhumal, D. Treffer, et al., Concordance of vacuum compression molding with spray drying in screening of amorphous solid dispersions of itraconazole, Int. J. Pharm. 654 (2024) 123952.

[27] B. Brandl, S. Eder, et al., Toward high-resolution 3D-printing of pharmaceutical implants – a holistic analysis of relevant material properties and process parameters, Int. J. Pharm. 660 (2024) 124356.

[28] L. Krueger, A. Awad, et al., Clinical translation of 3D printed pharmaceuticals, Nat. Rev. Bioeng. 2 (2024) 801–803.

[29] R.L. Milliken, T. Quinten, et al., Application of 3D printing in early phase development of pharmaceutical solid dosage forms, Int. J. Pharm. 653 (2024) 123902.

[30] A.K. Jørgensen, J.J. Ong, et al., Advancing non-destructive analysis of 3D printed medicines, Trends Pharmacol. Sci. 44 (6) (2023) 379–393.

[31] Agency MHpR, Consultation on Point of Care Manufacturing: Consultation Outcome, 2023.

[32] Administration USFD, Distributed Manufacturing and Point-of-Care Manufacturing of Drugs - Discussion Paper. Silver Spring, Maryland 20993, US, 2022.

[33] Administration USFD, 3D Printing Medical Devices at the Point of Care: Discussion Paper, 2021.

[34] Quality Innovation Group EMA, Fourth listen-and-learn focus group meeting of the Quality Innovation Group, 2024.

[35] Commission E, Conformity Assessment Procedures for 3D Printing and 3D Printed Products to be Used in Medical Context for COVID-19, 2020.

[36] S.J. Trenfield, P. Januskaite, et al., Prediction of solid-state form of SLS 3D printed medicines using NIR and Raman spectroscopy, Pharmaceutics 14 (3) (2022) 589.

[37] S.J. Trenfield, X. Xu, et al., Releasing fast and slow: non-destructive prediction of density and drug release from SLS 3D printed tablets using NIR spectroscopy, Int. J. Pharm. X 5 (2023) 100148.

[38] T.P. Forbes, J.G. Gillen, et al., Quality by design considerations for drop-on-demand point-of-care pharmaceutical manufacturing of precision medicine, Mol. Pharm. 21 (7) (2024) 3268–3280.

[39] T.L. Yang, M. Stogiannari, et al., Towards point-of-care manufacturing and analysis of immediate-release 3D printed hydrocortisone tablets for the treatment of congenital adrenal hyperplasia, Int. J. Pharm. 642 (2023) 123072.

[40] I. Seoane-Viaño, X. Xu, et al., A case study on decentralized manufacturing of 3D printed medicines, Int. J. Pharm. X 5 (2023) 100184.

[41] M. Edinger, L.-D. Iftimi, et al., Quantification of inkjet-printed pharmaceuticals on porous substrates using Raman spectroscopy and near-infrared spectroscopy, AAPS PharmSciTech 20 (5) (2019) 207.

[42] T.L. Yang, J. Szewc, et al., The use of near-infrared as process analytical technology (PAT) during 3D printing tablets at the point-of-care, Int. J. Pharm. 642 (2023) 123073.

[43] C.W.H. Chan, B.M.H. Law, et al., Pharmacogenomics of breast cancer: highlighting CYP2D6 and tamoxifen, J. Cancer Res. Clin. Oncol. 146 (6) (2020) 1395–1404.

[44] S. Henry, A. Samaro, et al., Extrusion-based 3D printing of oral solid dosage forms: material requirements and equipment dependencies, Int. J. Pharm. 598 (2021) 120361.

[45] H. Windolf, R. Chamberlain, et al., Predicting drug release from 3D printed oral medicines based on the surface area to volume ratio of tablet geometry, Pharmaceutics [Internet] 13 (9) (2021).

[46] E. Prasad, M.T. Islam, et al., Development of a hot-melt extrusion (HME) process to produce drug loaded Affinisol™ 15LV filaments for fused filament fabrication (FFF) 3D printing, Addit. Manuf. 29 (2019) 100776.

[47] V.A. Dubinsksaya, N.A. Polyakov, et al., Studies of moisture exchange between stearic acid, calcium stearate, and magnesium stearate, Pharm. Chem. J. 44 (2) (2010) 89–93.

[48] T.N. Hiew, N.A.B. Johan, et al., Effect of moisture sorption on the performance of crospovidone, Int. J. Pharm. 514 (1) (2016) 322–331.

[49] J. Li, Y. Wu, Lubricants in pharmaceutical solid dosage forms, Lubricants [Internet] 2 (1) (2014) 21–43.

[50] P. Okoye, S.H. Wu, et al., To evaluate the effect of various magnesium stearate polymorphs using powder rheology and thermal analysis, Drug Dev. Ind. Pharm. 38 (12) (2012) 1470–1478.

[51] S.P. Delaney, M.J. Nethercott, et al., Characterization of synthesized and commercial forms of magnesium stearate using differential scanning calorimetry, thermogravimetric analysis, powder X-ray diffraction, and solid-state NMR spectroscopy, J. Pharm. Sci. 106 (1) (2017) 338–347.

[52] A. Mojiri, N. Grbac, et al., D-mannitol for medium temperature thermal energy storage, Sol. Energy Mater. Sol. Cells 176 (2018) 150–156.

[53] N.N. Mohammed, S. Majumdar, et al., Klucel™ EF and ELF polymers for immediate-release oral dosage forms prepared by melt extrusion technology, AAPS PharmSciTech 13 (4) (2012) 1158–1169.

[54] S. Nakanishi, M. Fujii, et al., Evaluation of the physicochemical characteristics of crospovidone that influence solid dispersion preparation, Int. J. Pharm. 413 (1) (2011) 119–125.

[55] I. Goldberg, Y. Becker, Polymorphs of tamoxifen citrate: detailed structural characterization of the stable form, J. Pharm. Sci. 76 (3) (1987) 259–264.

[56] M.C. Gamberini, C. Baraldi, et al., Vibrational study of tamoxifen citrate polymorphism, J. Mol. Struct. 840 (1) (2007) 29–37.

[57] P. Zarmpi, T. Flanagan, et al., Biopharmaceutical aspects and implications of excipient variability in drug product performance, Eur. J. Pharm. Biopharm. 111 (2017) 1–15.

[58] E. Książek, Citric acid: properties, microbial production, and applications in industries, Molecules 29 (1) (2023).

[59] L. Denis, A.K. Jørgensen, et al., Developing an innovative 3D printing platform for production of personalised medicines in a hospital for the OPERA clinical trial, Int. J. Pharm. 661 (2024) 124306.

[60] Z.A. Parray, M.I. Hassan, et al., Amphiphilic nature of polyethylene glycols and their role in medical research, Polym. Test. 82 (2020) 106316.

[61] N. SreeHarsha, J.G. Hiremath, et al., An approach to enhance dissolution rate of tamoxifen citrate, Biomed. Res. Int. 2019 (2019) 2161348.

[62] S. Omari, E.A. Ashour, et al., Formulation development of loratadine immediate-release tablets using hot-melt extrusion and 3D printing technology, J. Drug Deliv. Sci. Technol. 74 (2022) 103505.

[63] S.J. Trenfield, A. Goyanes, et al., 3D printed drug products: non-destructive dose verification using a rapid point-and-shoot approach, Int. J. Pharm. 549 (1) (2018) 283–292.

[64] J.J. Ong, A.K. Jørgensen, et al., Volumetric printing and non-destructive drug quantification of water-soluble supramolecular hydrogels, Drug Deliv. Transl. Res. (2024) 1–16.

[65] Å. Rinnan, F.V.D. Berg, et al., Review of the most common pre-processing techniques for near-infrared spectra, TrAC Trends Anal. Chem. 28 (10) (2009) 1201–1222.

[66] R.J. Barnes, M.S. Dhanoa, et al., Standard normal variate transformation and de-trending of near-infrared diffuse reflectance spectra, Appl. Spectrosc. 43 (5) (1989) 772–777.

[67] J.M. Roger, A. Mallet, et al., Preprocessing NIR spectra for aquaphotomics, Molecules 27 (2022) 20.

[68] C. Bendicho-Lavilla, L. Rodríguez-Pombo, et al., Ensuring the quality of 3D printed medicines: integrating a balance into a pharmaceutical printer for in-line uniformity of mass testing, J. Drug Deliv. Sci. Technol. 92 (2024) 105337.